BELLE-CONF-0435
ICHEP04 6-0681

New Measurements of Time-Dependent CP-Violating Asymmetries in $b \to s$ Transitions at Belle

K. Abe,[10] K. Abe,[46] N. Abe,[49] I. Adachi,[10] H. Aihara,[48] M. Akatsu,[24] Y. Asano,[53] T. Aso,[52] V. Aulchenko,[2] T. Aushev,[14] T. Aziz,[44] S. Bahinipati,[6] A. M. Bakich,[43] Y. Ban,[36] M. Barbero,[9] A. Bay,[20] I. Bedny,[2] U. Bitenc,[15] I. Bizjak,[15] S. Blyth,[29] A. Bondar,[2] A. Bozek,[30] M. Bračko,[22,15] J. Brodzicka,[30] T. E. Browder,[9] M.-C. Chang,[29] P. Chang,[29] Y. Chao,[29] A. Chen,[26] K.-F. Chen,[29] W. T. Chen,[26] B. G. Cheon,[4] R. Chistov,[14] S.-K. Choi,[8] Y. Choi,[42] Y. K. Choi,[42] A. Chuvikov,[37] S. Cole,[43] M. Danilov,[14] M. Dash,[55] L. Y. Dong,[12] R. Dowd,[23] J. Dragic,[23] A. Drutskoy,[6] S. Eidelman,[2] Y. Enari,[24] D. Epifanov,[2] C. W. Everton,[23] F. Fang,[9] S. Fratina,[15] H. Fujii,[10] N. Gabyshev,[2] A. Garmash,[37] T. Gershon,[10] A. Go,[26] G. Gokhroo,[44] B. Golob,[21,15] M. Grosse Perdekamp,[38] H. Guler,[9] J. Haba,[10] F. Handa,[47] K. Hara,[10] T. Hara,[34] N. C. Hastings,[10] K. Hasuko,[38] K. Hayasaka,[24] H. Hayashii,[25] M. Hazumi,[10] E. M. Heenan,[23] I. Higuchi,[47] T. Higuchi,[10] L. Hinz,[20] T. Hojo,[34] T. Hokuue,[24] Y. Hoshi,[46] K. Hoshina,[51] S. Hou,[26] W.-S. Hou,[29] Y. B. Hsiung,[29] H.-C. Huang,[29] T. Igaki,[24] Y. Igarashi,[10] T. Iijima,[24] A. Imoto,[25] K. Inami,[24] A. Ishikawa,[10] H. Ishino,[49] K. Itoh,[48] R. Itoh,[10] M. Iwamoto,[3] M. Iwasaki,[48] Y. Iwasaki,[10] R. Kagan,[14] H. Kakuno,[48] J. H. Kang,[56] J. S. Kang,[17] P. Kapusta,[30] S. U. Kataoka,[25] N. Katayama,[10] H. Kawai,[3] H. Kawai,[48] Y. Kawakami,[24] N. Kawamura,[1] T. Kawasaki,[32] N. Kent,[9] H. R. Khan,[49] A. Kibayashi,[49] H. Kichimi,[10] H. J. Kim,[19] H. O. Kim,[42] Hyunwoo Kim,[17] J. H. Kim,[42] S. K. Kim,[41] T. H. Kim,[56] K. Kinoshita,[6] P. Koppenburg,[10] S. Korpar,[22,15] P. Križan,[21,15] P. Krokovny,[2] R. Kulasiri,[6] C. C. Kuo,[26] H. Kurashiro,[49] E. Kurihara,[3] A. Kusaka,[48] A. Kuzmin,[2] Y.-J. Kwon,[56] J. S. Lange,[7] G. Leder,[13] S. E. Lee,[41] S. H. Lee,[41] Y.-J. Lee,[29] T. Lesiak,[30] J. Li,[40] A. Limosani,[23] S.-W. Lin,[29] D. Liventsev,[14] J. MacNaughton,[13] G. Majumder,[44] F. Mandl,[13] D. Marlow,[37] T. Matsuishi,[24] H. Matsumoto,[32] S. Matsumoto,[5] T. Matsumoto,[50] A. Matyja,[30] Y. Mikami,[47] W. Mitaroff,[13] K. Miyabayashi,[25] Y. Miyabayashi,[24] H. Miyake,[34] H. Miyata,[32] R. Mizuk,[14] D. Mohapatra,[55] G. R. Moloney,[23] G. F. Moorhead,[23] T. Mori,[49] A. Murakami,[39] T. Nagamine,[47] Y. Nagasaka,[11] T. Nakadaira,[48] I. Nakamura,[10] E. Nakano,[33] M. Nakao,[10] H. Nakazawa,[10] Z. Natkaniec,[30] K. Neichi,[46] S. Nishida,[10] O. Nitoh,[51] S. Noguchi,[25] T. Nozaki,[10] A. Ogawa,[38] S. Ogawa,[45] T. Ohshima,[24] T. Okabe,[24] S. Okuno,[16] S. L. Olsen,[9] Y. Onuki,[32] W. Ostrowicz,[30] H. Ozaki,[10] P. Pakhlov,[14] H. Palka,[30] C. W. Park,[42] H. Park,[19] K. S. Park,[42] N. Parslow,[43] L. S. Peak,[43] M. Pernicka,[13] J.-P. Perroud,[20] M. Peters,[9] L. E. Piilonen,[55] A. Poluektov,[2] F. J. Ronga,[10] N. Root,[2] M. Rozanska,[30] H. Sagawa,[10] M. Saigo,[47] S. Saitoh,[10] Y. Sakai,[10] H. Sakamoto,[18] T. R. Sarangi,[10] M. Satapathy,[54] N. Sato,[24] O. Schneider,[20] J. Schümann,[29] C. Schwanda,[13] A. J. Schwartz,[6] T. Seki,[50] S. Semenov,[14] K. Senyo,[24] Y. Settai,[5] R. Seuster,[9] M. E. Sevior,[23] T. Shibata,[32] H. Shibuya,[45] B. Shwartz,[2] V. Sidorov,[2] V. Siegle,[38] J. B. Singh,[35] A. Somov,[6] N. Soni,[35] R. Stamen,[10] S. Stanič,[53,*] M. Starič,[15] A. Sugi,[24] A. Sugiyama,[39] K. Sumisawa,[34] T. Sumiyoshi,[50] S. Suzuki,[39] S. Y. Suzuki,[10] O. Tajima,[10] F. Takasaki,[10] K. Tamai,[10] N. Tamura,[32] K. Tanabe,[48] M. Tanaka,[10] G. N. Taylor,[23]

Y. Teramoto,[33] X. C. Tian,[36] S. Tokuda,[24] S. N. Tovey,[23] K. Trabelsi,[9] T. Tsuboyama,[10] T. Tsukamoto,[10] K. Uchida,[9] S. Uehara,[10] T. Uglov,[14] K. Ueno,[29] Y. Unno,[3] S. Uno,[10] Y. Ushiroda,[10] G. Varner,[9] K. E. Varvell,[43] S. Villa,[20] C. C. Wang,[29] C. H. Wang,[28] J. G. Wang,[55] M.-Z. Wang,[29] M. Watanabe,[32] Y. Watanabe,[49] L. Widhalm,[13] Q. L. Xie,[12] B. D. Yabsley,[55] A. Yamaguchi,[47] H. Yamamoto,[47] S. Yamamoto,[50] T. Yamanaka,[34] Y. Yamashita,[31] M. Yamauchi,[10] Heyoung Yang,[41] P. Yeh,[29] J. Ying,[36] K. Yoshida,[24] Y. Yuan,[12] Y. Yusa,[47] H. Yuta,[1] S. L. Zang,[12] C. C. Zhang,[12] J. Zhang,[10] L. M. Zhang,[40] Z. P. Zhang,[40] V. Zhilich,[2] T. Ziegler,[37] D. Žontar,[21,15] and D. Zürcher[20]

(The Belle Collaboration)

[1]*Aomori University, Aomori*
[2]*Budker Institute of Nuclear Physics, Novosibirsk*
[3]*Chiba University, Chiba*
[4]*Chonnam National University, Kwangju*
[5]*Chuo University, Tokyo*
[6]*University of Cincinnati, Cincinnati, Ohio 45221*
[7]*University of Frankfurt, Frankfurt*
[8]*Gyeongsang National University, Chinju*
[9]*University of Hawaii, Honolulu, Hawaii 96822*
[10]*High Energy Accelerator Research Organization (KEK), Tsukuba*
[11]*Hiroshima Institute of Technology, Hiroshima*
[12]*Institute of High Energy Physics, Chinese Academy of Sciences, Beijing*
[13]*Institute of High Energy Physics, Vienna*
[14]*Institute for Theoretical and Experimental Physics, Moscow*
[15]*J. Stefan Institute, Ljubljana*
[16]*Kanagawa University, Yokohama*
[17]*Korea University, Seoul*
[18]*Kyoto University, Kyoto*
[19]*Kyungpook National University, Taegu*
[20]*Swiss Federal Institute of Technology of Lausanne, EPFL, Lausanne*
[21]*University of Ljubljana, Ljubljana*
[22]*University of Maribor, Maribor*
[23]*University of Melbourne, Victoria*
[24]*Nagoya University, Nagoya*
[25]*Nara Women's University, Nara*
[26]*National Central University, Chung-li*
[27]*National Kaohsiung Normal University, Kaohsiung*
[28]*National United University, Miao Li*
[29]*Department of Physics, National Taiwan University, Taipei*
[30]*H. Niewodniczanski Institute of Nuclear Physics, Krakow*
[31]*Nihon Dental College, Niigata*
[32]*Niigata University, Niigata*
[33]*Osaka City University, Osaka*
[34]*Osaka University, Osaka*
[35]*Panjab University, Chandigarh*
[36]*Peking University, Beijing*

[37]Princeton University, Princeton, New Jersey 08545
[38]RIKEN BNL Research Center, Upton, New York 11973
[39]Saga University, Saga
[40]University of Science and Technology of China, Hefei
[41]Seoul National University, Seoul
[42]Sungkyunkwan University, Suwon
[43]University of Sydney, Sydney NSW
[44]Tata Institute of Fundamental Research, Bombay
[45]Toho University, Funabashi
[46]Tohoku Gakuin University, Tagajo
[47]Tohoku University, Sendai
[48]Department of Physics, University of Tokyo, Tokyo
[49]Tokyo Institute of Technology, Tokyo
[50]Tokyo Metropolitan University, Tokyo
[51]Tokyo University of Agriculture and Technology, Tokyo
[52]Toyama National College of Maritime Technology, Toyama
[53]University of Tsukuba, Tsukuba
[54]Utkal University, Bhubaneswer
[55]Virginia Polytechnic Institute and State University, Blacksburg, Virginia 24061
[56]Yonsei University, Seoul

(Dated: February 7, 2008)

Abstract

We present new measurements of CP-violation parameters in $B^0 \to \phi K^0$, $K^+K^-K^0_S$, $f_0(980)K^0_S$, $\eta' K^0_S$, ωK^0_S, $K^0_S\pi^0$, and $K^{*0}\gamma$ ($K^{*0} \to K^0_S\pi^0$) decays based on a sample of 275×10^6 $B\overline{B}$ pairs collected at the $\Upsilon(4S)$ resonance with the Belle detector at the KEKB energy-asymmetric e^+e^- collider. One neutral B meson is fully reconstructed in one of the specified decay channels, and the flavor of the accompanying B meson is identified from its decay products. CP-violation parameters for each of the decay modes are obtained from the asymmetries in the distributions of the proper-time intervals between the two B decays. All results are preliminary.

PACS numbers: 11.30.Er, 12.15.Hh, 13.25.Hw

*on leave from Nova Gorica Polytechnic, Nova Gorica

I. INTRODUCTION

The phenomena of CP violation in the flavor-changing $b \to s$ transition are sensitive to physics at a very high-energy scale [1]. Theoretical studies indicate that large deviations from standard model (SM) expectations are allowed for time-dependent CP asymmetries in B^0 meson decays [2]. Experimental investigations have recently been launched at the two B factories, each of which has produced more than 10^8 $B\overline{B}$ pairs. Belle's previous measurement of the $B^0 \to \phi K^0_S$ decay [3], which is dominated by the $b \to s\overline{s}s$ transition, yielded a value that differs from the SM expectation by 3.5 standard deviations [4]. Measurements with a larger data sample are required to elucidate this difference. It is also essential to examine additional modes that may be sensitive to the same $b \to s$ penguin amplitude. In this spirit, experimental results using the decay modes $B^0 \to \phi K^0_L$, $K^+K^-K^0_S$, $f_0(980)K^0_S$, $\eta' K^0_S$, and $K^0_S\pi^0$ have already been reported [4, 5].

In the SM, CP violation arises from an irreducible phase, the Kobayashi-Maskawa (KM) phase [7], in the weak-interaction quark-mixing matrix. In particular, the SM predicts CP asymmetries in the time-dependent rates for B^0 and $\overline{B}^0$ decays to a common CP eigenstate f_{CP} [8]. In the decay chain $\Upsilon(4S) \to B^0\overline{B}^0 \to f_{CP}f_{\rm tag}$, where one of the B mesons decays at time t_{CP} to a final state f_{CP} and the other decays at time $t_{\rm tag}$ to a final state $f_{\rm tag}$ that distinguishes between B^0 and $\overline{B}^0$, the decay rate has a time dependence given by

$$\mathcal{P}(\Delta t) = \frac{e^{-|\Delta t|/\tau_{B^0}}}{4\tau_{B^0}}\Big\{1 + q\cdot\Big[\mathcal{S}\sin(\Delta m_d\Delta t) + \mathcal{A}\cos(\Delta m_d\Delta t)\Big]\Big\}. \quad (1)$$

Here $\mathcal{S}$ and $\mathcal{A}$ are CP-violation parameters, τ_{B^0} is the B^0 lifetime, Δm_d is the mass difference between the two B^0 mass eigenstates, $\Delta t = t_{CP} - t_{\rm tag}$, and the b-flavor charge $q = +1$ (-1) when the tagging B meson is a B^0 ($\overline{B}^0$). To a good approximation, the SM predicts $\mathcal{S} = -\xi_f \sin 2\phi_1$, where $\xi_f = +1(-1)$ corresponds to CP-even (-odd) final states, and $\mathcal{A} = 0$ for both $b \to c\overline{c}s$ and $b \to s\overline{s}s$ transitions. Recent measurements of time-dependent CP asymmetries in $B^0 \to J/\psi K^0_S$ and related decay modes, which are governed by the $b \to c\overline{c}s$ transition, by Belle [9, 10] and BaBar [11] already determine $\sin 2\phi_1$ rather precisely; the present world average value is $\sin 2\phi_1 = +0.726 \pm 0.037$ [6]. This serves as a firm reference point for the SM.

Belle's previous measurements for $B^0 \to \phi K^0_S$, $K^+K^-K^0_S$ and $\eta' K^0_S$ were based on a 140 fb^{-1} data sample (DS-I) containing 152×10^6 $B\overline{B}$ pairs. While ϕK^0_S and $\eta' K^0_S$ final states are CP eigenstates with $\xi_f = -1$, the $K^+K^-K^0_S$ final state is in general a mixture of both $\xi_f = +1$ and -1. Excluding K^+K^- pairs that are consistent with a $\phi \to K^+K^-$ decay from the $B^0 \to K^+K^-K^0_S$ sample, we find that the $K^+K^-K^0_S$ state is primarily $\xi_f = +1$; a measurement of the $\xi_f = +1$ fraction with DS-I gives $1.03 \pm 0.15({\rm stat}) \pm 0.05({\rm syst})$ [4]. In the following determination of $\mathcal{S}$ and $\mathcal{A}$, we fix $\xi_f = +1$ for this mode.

In this report, we describe improved measurements incorporating an additional 113 fb^{-1} data sample that contains 123×10^6 $B\overline{B}$ pairs (DS-II) for a total of 275×10^6 $B\overline{B}$ pairs. We include additional ϕK^0_S and $\eta' K^0_S$ subdecay modes that were not used in the previous analysis. We also describe new measurements of CP asymmetries for the following CP-eigenstate B^0 decay modes: $B^0 \to \phi K^0_L$ and $f_0(980)K^0_S$ for $\xi_f = +1$; $B^0 \to \omega K^0_S$ and $K^0_S\pi^0$ for $\xi_f = -1$. The decays $B^0 \to \phi K^0_S$ and ϕK^0_L are combined in this analysis by redefining $\mathcal{S}$ as $-\xi_f\mathcal{S}$ to take the opposite CP parities into account, and are collectively called "$B^0 \to \phi K^0$". The CP asymmetries for the decay $B^0 \to \omega K^0_S$ are measured for the first time.

Finally, we also measure time-dependent CP violation in the decay $B^0 \to K^{*0}\gamma$ ($K^{*0} \to K^0_S\pi^0$) [12], which is not a CP eigenstate but is sensitive to physics beyond the SM [13]. Within the SM, the photon emitted from a B^0 ($\overline{B}^0$) meson is dominantly right-handed (left-handed). Therefore the polarization of the photon carries information on the original b-flavor; the decay is thus almost flavor-specific. The SM predicts a small asymmetry $\mathcal{S} \sim -2(m_s/m_b)\sin 2\phi_1$, where m_b (m_s) is the b-quark (s-quark) mass [13]. Any significant deviation from this expectation would be a manifestation of physics beyond the SM.

At the KEKB energy-asymmetric e^+e^- (3.5 on 8.0 GeV) collider [14], the $\Upsilon(4S)$ is produced with a Lorentz boost of $\beta\gamma = 0.425$ nearly along the electron beamline (z). Since the B^0 and $\overline{B}^0$ mesons are approximately at rest in the $\Upsilon(4S)$ center-of-mass system (cms), Δt can be determined from the displacement in z between the f_{CP} and $f_{\rm tag}$ decay vertices: $\Delta t \simeq (z_{CP} - z_{\rm tag})/(\beta\gamma c) \equiv \Delta z/(\beta\gamma c)$.

The Belle detector is a large-solid-angle magnetic spectrometer that consists of a silicon vertex detector (SVD), a 50-layer central drift chamber (CDC), an array of aerogel threshold Cherenkov counters (ACC), a barrel-like arrangement of time-of-flight scintillation counters (TOF), and an electromagnetic calorimeter comprised of CsI(Tl) crystals (ECL) located inside a superconducting solenoid coil that provides a 1.5 T magnetic field. An iron flux-return located outside of the coil is instrumented to detect K^0_L mesons and to identify muons (KLM). The detector is described in detail elsewhere [15]. Two inner detector configurations were used. A 2.0 cm radius beampipe and a 3-layer silicon vertex detector (SVD-I) were used for DS-I, while a 1.5 cm radius beampipe, a 4-layer silicon detector (SVD-II) and a small-cell inner drift chamber were used for DS-II [16].

II. EVENT SELECTION, FLAVOR TAGGING AND VERTEX RECONSTRUCTION

A. Overview

We reconstruct the following B^0 decay modes to measure CP asymmetries: $B^0 \to \phi K^0_S$, ϕK^0_L, $K^+K^-K^0_S$, $f_0(980)K^0_S$, $\eta' K^0_S$, ωK^0_S, $K^0_S\pi^0$, and $K^{*0}\gamma$ ($K^{*0} \to K^0_S\pi^0$). We exclude K^+K^- pairs that are consistent with a $\phi \to K^+K^-$ decay from the $B^0 \to K^+K^-K^0_S$ sample. The intermediate meson states are reconstructed from the following decays: $\pi^0 \to \gamma\gamma$, $K^0_S \to \pi^+\pi^-$ (also $\pi^0\pi^0$ for the ϕK^0_S decay), $\eta \to \gamma\gamma$ or $\pi^+\pi^-\pi^0$, $\rho^0 \to \pi^+\pi^-$, $\omega \to \pi^+\pi^-\pi^0$, $K^{*0} \to K^0_S\pi^0$, $\eta' \to \rho^0\gamma$ or $\eta\pi^+\pi^-$, $f_0(980) \to \pi^+\pi^-$, and $\phi \to K^+K^-$.

Among the decay chains listed above, $B^0 \to \phi K^0_S$ ($K^0_S \to \pi^+\pi^-$), $B^0 \to K^+K^-K^0_S$, $B^0 \to \eta' K^0_S$ ($\eta' \to \rho^0\gamma$), and $B^0 \to \eta' K^0_S$ ($\eta' \to \eta\pi^+\pi^-$, $\eta \to \gamma\gamma$) decays were used in the previous analysis [4]. The selection criteria for these decays remain the same. For the other B^0 decay modes that are now included, identification of photons, neutral and charged kaons, and neutral and charged pions is based on the procedure used previously. However, the selection criteria for each B^0 decay mode were optimized individually and are thus different from one another.

B. $B^0 \to \phi K^0_S$ and $K^+K^-K^0_S$

We use well-reconstructed charged tracks with a sufficient number of associated hits in the CDC. Charged kaons and pions except for those from $K^0_S \to \pi^+\pi^-$ decays are required

to originate from the interaction point (IP). We distinguish charged kaons from pions based on a kaon (pion) likelihood $\mathcal{L}_{K(\pi)}$ derived from the TOF, ACC and dE/dx measurements in the CDC.

Pairs of oppositely charged tracks that have an invariant mass within 0.030 GeV/c^2 of the nominal K^0_S mass are used to reconstruct $K^0_S \to \pi^+\pi^-$ decays. The $\pi^+\pi^-$ vertex is required to be displaced from the IP by a minimum transverse distance of 0.22 cm for high momentum (> 1.5 GeV/c) candidates and 0.08 cm for those with momentum less than 1.5 GeV/c. The direction of the pion pair momentum must also agree with the direction defined by the IP and the vertex displacement within 0.03 rad for high-momentum candidates, and within 0.1 rad for the remaining candidates.

Photons are identified as isolated ECL clusters that are not matched to any charged track. To select $K^0_S \to \pi^0\pi^0$ decays, we reconstruct π^0 candidates from pairs of photons with $E_\gamma > 0.05$ GeV, where E_γ is the photon energy measured with the ECL. The reconstructed π^0 candidate is required to have an invariant mass between 0.08 and 0.15 GeV/c^2 and a momentum above 0.1 GeV/c. The large mass range is used to achieve a high reconstruction efficiency. Candidate $K^0_S \to \pi^0\pi^0$ decays are required to have invariant masses between 0.47 GeV/c^2 and 0.52 GeV/c^2, where we perform a fit with constraints on the K^0_S vertex and the π^0 masses to improve the $\pi^0\pi^0$ invariant mass resolution. We also require that the distance between the IP and the reconstructed K^0_S decay vertex be larger than -10 cm, where the positive direction is defined by the K^0_S momentum.

Candidate $\phi \to K^+K^-$ decays are required to have a K^+K^- invariant mass that is within 0.01 GeV/c^2 of the nominal ϕ meson mass. Since the ϕ meson selection is effective in reducing background events, we impose only minimal kaon-identification requirements; $\mathcal{R}_{K/\pi} \equiv \mathcal{L}_K/(\mathcal{L}_K + \mathcal{L}_\pi) > 0.1$ is required, where the kaon likelihood ratio $\mathcal{R}_{K/\pi}$ has values between 0 (likely to be a pion) and 1 (likely to be a kaon). We use a more stringent kaon-identification requirement, $\mathcal{R}_{K/\pi} > 0.6$, to select non-resonant K^+K^- candidates for the decay $B^0 \to K^+K^-K^0_S$. We reject K^+K^- pairs that are consistent with $D^0 \to K^+K^-$, $\chi_{c0} \to K^+K^-$, or $J/\psi \to K^+K^-$ decays. We also remove $D^+ \to K^0_S K^+$ candidates.

For reconstructed $B \to f_{CP}$ candidates, we identify B meson decays using the energy difference $\Delta E \equiv E_B^{\rm cms} - E_{\rm beam}^{\rm cms}$ and the beam-energy constrained mass $M_{\rm bc} \equiv \sqrt{(E_{\rm beam}^{\rm cms})^2 - (p_B^{\rm cms})^2}$, where $E_{\rm beam}^{\rm cms}$ is the beam energy in the cms, and $E_B^{\rm cms}$ and $p_B^{\rm cms}$ are the cms energy and momentum of the reconstructed B candidate, respectively. The B meson signal region is defined as $|\Delta E| < 0.06$ GeV for $B^0 \to \phi K^0_S$ ($K^0_S \to \pi^+\pi^-$), -0.15 GeV $< \Delta E < 0.1$ GeV for $B^0 \to \phi K^0_S$ ($K^0_S \to \pi^0\pi^0$), $|\Delta E| < 0.04$ GeV for $B^0 \to K^+K^-K^0_S$, and 5.27 GeV/$c^2 < M_{\rm bc} < 5.29$ GeV/c^2 for all decays.

The dominant background to the $B^0 \to \phi K^0_S$ decay comes from $e^+e^- \to u\overline{u}$, $d\overline{d}$, $s\overline{s}$, or $c\overline{c}$ continuum events. Since these tend to be jet-like, while the signal events tend to be spherical, we use a set of variables that characterize the event topology to distinguish between the two. We combine $S_\perp$, θ_T and modified Fox-Wolfram moments [17] into a Fisher discriminant $\mathcal{F}$, where $S_\perp$ is the scalar sum of the transverse momenta of all particles outside a 45° cone around the candidate ϕ meson direction divided by the scalar sum of their total momenta, and θ_T is the angle between the thrust axis of the B candidate and that of the other particles in the cms. We also use the angle of the reconstructed B^0 candidate with respect to the beam direction in the cms (θ_B), and the helicity angle θ_H defined as the angle between the B^0 meson momentum and the daughter K^+ momentum in the ϕ meson rest frame. We combine $\mathcal{F}$, $\cos\theta_B$ and $\cos\theta_H$ into a signal [background] likelihood variable, which is defined as $\mathcal{L}_{\rm sig[bkg]} \equiv \mathcal{L}_{\rm sig[bkg]}(\mathcal{F}) \times \mathcal{L}_{\rm sig[bkg]}(\cos\theta_B) \times \mathcal{L}_{\rm sig[bkg]}(\cos\theta_H)$. We impose

requirements on the likelihood ratio $\mathcal{R}_{\rm s/b} \equiv \mathcal{L}_{\rm sig}/(\mathcal{L}_{\rm sig} + \mathcal{L}_{\rm bkg})$ to maximize the figure-of-merit (FoM) defined as $N_{\rm sig}^{\rm MC}/\sqrt{N_{\rm sig}^{\rm MC} + N_{\rm bkg}}$, where $N_{\rm sig}^{\rm MC}$ ($N_{\rm bkg}$) represents the expected number of signal (background) events in the signal region. We estimate $N_{\rm sig}^{\rm MC}$ using Monte Carlo (MC) events, while $N_{\rm bkg}$ is determined from events outside the signal region. The requirement for $\mathcal{R}_{\rm s/b}$ depends both on the decay mode and on the flavor-tagging quality, r, which is described in Sec. III. The threshold values range from 0.1 (used for $r > 0.875$) to 0.4 (used for $r < 0.25$) for the decay $B^0 \to \phi K_S^0$ ($K_S^0 \to \pi^+\pi^-$), and from 0.25 to 0.65 for the decay $B^0 \to K^+K^-K_S^0$. We impose a more stringent requirement, $\mathcal{R}_{\rm s/b} > 0.75$, for all r values in the decay $B^0 \to \phi K_S^0$ ($K_S^0 \to \pi^0\pi^0$).

We use events outside the signal region as well as a large MC sample to study the background components. The dominant background is from continuum. The contributions from $B\overline{B}$ events are small. The contamination of $B^0 \to K^+K^-K_S^0$ events in the $B^0 \to \phi K_S^0$ sample is $7.1 \pm 1.6\%$ ($6.2 \pm 2.0\%$) for DS-I (DS-II). Backgrounds from the decay $B^0 \to f_0(980)K_S^0$ ($f_0(980) \to K^+K^-$), which has a CP eigenvalue opposite to ϕK_S^0, are found to be $0.4^{+1.9}_{-0.4}\%$ ($0.0^{+2.0}_{-0.0}\%$) for DS-I (DS-II). The influence of these backgrounds is treated as a source of systematic uncertainty.

Figure 1(a) and (c) show the $M_{\rm bc}$ distribution for the reconstructed $B^0 \to \phi K_S^0$ and $K^+K^-K_S^0$ candidates within the ΔE signal regions after flavor tagging and vertex reconstruction. The signal yield is determined from an unbinned two-dimensional maximum-likelihood fit to the ΔE-$M_{\rm bc}$ distribution in the fit region defined as $5.2\ {\rm GeV}/c^2 < M_{\rm bc} < 5.3\ {\rm GeV}/c^2$ for all modes, and $-0.12\ {\rm GeV} < \Delta E < 0.25\ {\rm GeV}$ for the $B^0 \to \phi K_S^0$ ($K_S^0 \to \pi^+\pi^-$) or $K^+K^-K_S^0$ decay and $-0.15\ {\rm GeV} < \Delta E < 0.25\ {\rm GeV}$ for the $B^0 \to \phi K_S^0$ ($K_S^0 \to \pi^0\pi^0$) decay. The ϕK_S^0 ($K_S^0 \to \pi^+\pi^-$) signal distribution is modeled with a Gaussian function (a sum of two Gaussian functions) for $M_{\rm bc}$ (ΔE). The ϕK_S^0 ($K_S^0 \to \pi^0\pi^0$) signal distribution is modeled with a smoothed histogram obtained from MC events. For the continuum background, we use the ARGUS parameterization [18] for $M_{\rm bc}$ and a linear function for ΔE. The fits yield 139 ± 14 $B^0 \to \phi K_S^0$ events and 399 ± 28 $B^0 \to K^+K^-K_S^0$ events in the signal region, where the errors are statistical only.

C. $B^0 \to \phi K_L^0$

Candidate $\phi \to K^+K^-$ decays are selected with the same criteria as described above. We select K_L^0 candidates based on KLM and ECL information. There are two classes of K_L^0 candidates that we refer to as KLM and ECL candidates. The requirements for the KLM candidates are the same as those used in the $B^0 \to J/\psi K_L^0$ selection for the $\sin 2\phi_1$ measurement [9]. ECL candidates are selected from ECL clusters using a K_L^0 likelihood ratio [9], which is calculated from the following information: the distance between the ECL cluster and the closest extrapolated charged track position; the ECL cluster energy; E_9/E_{25}, the ratio of energies summed in 3×3 and 5×5 arrays of CsI(Tl) crystals surrounding the crystal at the center of the shower; the ECL shower width and the invariant mass of the shower. The likelihood ratio is required to be greater than 0.8. For both KLM and ECL candidates, we also require that the cosine of the angle between the K_L^0 direction and the direction of the missing momentum of the event in the laboratory frame be greater than 0.6.

Since the energy of the K_L^0 is not measured, $M_{\rm bc}$ and ΔE cannot be calculated in the same way that is used for the other final states. Using the four-momentum of a reconstructed ϕ candidate and the K_L^0 flight direction, we calculate the momentum of the K_L^0 candidate

requiring $\Delta E = 0$. We then calculate $p_B^{\rm cms}$, the momentum of the B candidate in the cms, and define the B meson signal region as 0.2 GeV/c $< p_B^{\rm cms} <$ 0.5 GeV/c. We impose the requirement $\mathcal{R}_{\rm s/b} > 0.98$ to reduce the continuum background. Here $\mathcal{R}_{\rm s/b}$ is based on the discriminating variables used for the $B^0 \to \phi K_S^0$ decay and the number of tracks originating from the IP with a momentum above 0.1 GeV/c. The $\mathcal{R}_{\rm s/b}$ requirement is chosen to optimize the FoM, which is calculated taking the background from both continuum and generic B decays into account. The K_L^0 detection efficiency difference between data and MC is studied using the decay $B^0 \to J/\psi K_L^0$, and corrections are applied to the $B^0 \to \phi K_L^0$ MC events to calculate the FoM. If there is more than one candidate $B^0 \to \phi K_L^0$ decay in the signal region, we take the one with the highest $\mathcal{R}_{\rm s/b}$ value. ECL candidates are not used if there is a candidate $B^0 \to \phi K_L^0$ decay with a KLM candidate. We find that about 90% of signal events are reconstructed with KLM candidates.

We study the background components using a large MC sample as well as data taken with cms energy 60 MeV below the nominal $\Upsilon(4S)$ mass (off-resonance data). The dominant background is from continuum. A MC study with the efficiency correction obtained from $B^0 \to J/\psi K_L^0$ data yields 9 ± 5 background events from B decays, which include $B^0 \to \phi K^{*0}$, ϕK_S^0 and $B^+ \to \phi K^{*+}$ decays. The influence of these backgrounds, including their CP asymmetries, is treated as a source of systematic uncertainty.

The $p_B^{\rm cms}$ distribution after flavor tagging and vertex reconstruction is shown in Fig. 1(b). The signal yield is determined from an extended unbinned maximum-likelihood fit in the range 0 GeV/c $< p_B^{\rm cms} <$ 1 GeV/c. The $B^0 \to \phi K_L^0$ signal shape is obtained from MC events. Background from $B\overline{B}$ pairs is also modeled with MC. We fix the ratio between the signal yield and the $B\overline{B}$ background based on known branching fractions and reconstruction efficiencies; uncertainty in the ratio is treated as a source of systematic error. The continuum background distribution is represented by a smoothed histogram obtained from MC events; we confirm that the function describes the off-resonance data well. The fit yields $36 \pm 15 \pm 10$ $B^0 \to \phi K_L^0$ events, where the first error is statistical and the second error is systematic. The sources of the systematic error include uncertainties in the efficiency corrections, in $B\overline{B}$ background branching fractions and in the background parameterizations. The result is in good agreement with the expected $B^0 \to \phi K_L^0$ signal yield (36 ± 9 events) obtained from MC after applying the efficiency correction from the $B^0 \to J/\psi K_L^0$ data.

D. $B^0 \to f_0(980) K_S^0$

Candidate $K_S^0 \to \pi^+\pi^-$ decays are selected with the criteria that are slightly different from those used for the $B^0 \to \phi K_S^0$ decay to obtain the best performance for the $B^0 \to f_0(980) K_S^0$ decay. Pairs of oppositely charged pions that have invariant masses between 0.890 and 1.088 GeV/c^2 are used to reconstruct $f_0(980) \to \pi^+\pi^-$ decays. Tracks that are identified as kaons ($\mathcal{R}_{K/\pi} > 0.7$) or electrons are not used. We require that both $K_S^0\pi^+$ and $K_S^0\pi^-$ combinations have invariant masses more than 0.1 GeV/c^2 above the nominal charged D meson mass; this removes background from $D^\pm \to K_S^0\pi^\pm$ and $K^{*\pm} \to K_S^0\pi^\pm$ decays.

The B meson signal region is defined as $|\Delta E| < 0.06$ GeV and 5.27 GeV/c^2 $< M_{\rm bc} <$ 5.29 GeV/c^2. The dominant background is from continuum. For the continuum suppression, we require $\mathcal{R}_{\rm s/b} > 0.6$ for events with the best-quality flavor tagging ($r > 0.875$), and $\mathcal{R}_{\rm s/b} > 0.8$ for other events. Here the signal likelihood ratio $\mathcal{R}_{\rm s/b}$ is obtained from $\cos\theta_B$ and $\mathcal{F}$, which consists of the modified Fox-Wolfram moments and $\cos\theta_T$.

Figure 1(d) shows the $M_{\rm bc}$ distribution for the reconstructed $B^0 \to f_0(980) K_S^0$ candidates

within the ΔE signal region after flavor tagging and vertex reconstruction. For the signal yield extraction, we first perform an unbinned two-dimensional maximum-likelihood fit to the ΔE-$M_{\rm bc}$ distribution in the fit region defined as 5.2 GeV/c^2 $< M_{\rm bc} <$ 5.3 GeV/c^2 and -0.3 GeV $< \Delta E <$ 0.4 GeV. The signal is modeled with a Gaussian function (a sum of two Gaussian functions) for $M_{\rm bc}$ (ΔE). For the continuum background, we use the ARGUS parameterization for $M_{\rm bc}$ and a linear function for ΔE. The fit yields the number of $B^0 \to \pi^+\pi^- K^0_S$ events that have $\pi^+\pi^-$ invariant masses within the $f_0(980)$ resonance region, which may include contributions from $B^0 \to \rho^0 K^0_S$ as well as non-resonant three-body $B^0 \to \pi^+\pi^- K^0_S$ decays. To separate these peaking backgrounds from the $B^0 \to f_0(980)K^0_S$ decay, we perform another fit to the $\pi^+\pi^-$ invariant mass distribution for the events inside the ΔE-$M_{\rm bc}$ signal region. We use Breit-Wigner functions for the $B^0 \to f_0(980)K^0_S$ signal as well as for $B^0 \to \rho K^0_S$ and a possible resonance above the $f_0(980)$ mass region [19]. Three-body $B^0 \to \pi^+\pi^- K^0_S$ decays are modeled with a fourth-order polynomial function. The other background is modeled with a threshold function. The fit yields 94 ± 14 $B^0 \to f_0(980)K^0_S$ events. The peaking background contribution in the ΔE-$M_{\rm bc}$ signal region is estimated to be 9 ± 3 events.

E. $B^0 \to \eta' K^0_S$

Candidate $K^0_S \to \pi^+\pi^-$ decays are selected with the same criteria as those used for the $B^0 \to \phi K^0_S$ decay. Charged pions from the η, ρ^0 or η' decay are selected from tracks originating from the IP. We reject kaon candidates by requiring $\mathcal{R}_{K/\pi} < 0.9$. Candidate photons from $\pi^0 \to \gamma\gamma$ decays are required to have $E_\gamma > 0.05$ GeV. The reconstructed π^0 candidate is required to satisfy 0.118 GeV/c^2 $< M_{\gamma\gamma} <$ 0.15 GeV/c^2 and $p^{\rm cms}_{\pi^0} > 0.1$ GeV/c, where $M_{\gamma\gamma}$ and $p^{\rm cms}_{\pi^0}$ are the invariant mass and the momentum in the cms, respectively. Candidate photons from $\eta \to \gamma\gamma$ ($\eta' \to \rho^0\gamma$) decays are required to have $E_\gamma > 0.05$ (0.1) GeV. The invariant mass of the photon pair is required to be between 0.5 and 0.57 GeV/c^2 for the $\eta \to \gamma\gamma$ decay. The $\pi^+\pi^-\pi^0$ invariant mass is required to be between 0.535 and 0.558 GeV/c^2 for the $\eta \to \pi^+\pi^-\pi^0$ decay. A kinematic fit with an η mass constraint is performed using the fitted vertex of the $\pi^+\pi^-$ tracks from the η' as the decay point. For $\eta' \to \rho^0\gamma$ decays, candidate ρ^0 mesons are reconstructed from pairs of vertex-constrained $\pi^+\pi^-$ tracks with an invariant mass between 0.55 and 0.92 GeV/c^2. The $\eta' \to \eta\pi^+\pi^-$ candidates are required to have a reconstructed mass between 0.94 and 0.97 GeV/c^2 (0.95 and 0.966 GeV/c^2) for the $\eta \to \gamma\gamma$ ($\eta \to \pi^+\pi^-\pi^0$) decay. Candidate $\eta' \to \rho^0\gamma$ decays are required to have a reconstructed mass from 0.935 to 0.975 GeV/c^2.

The B meson signal region is defined as $|\Delta E| < 0.06$ GeV for $B^0 \to \eta' K^0_S$ ($\eta' \to \rho^0\gamma$), -0.1 GeV $< \Delta E < 0.08$ GeV for $B^0 \to \eta' K^0_S$ ($\eta' \to \eta\pi^+\pi^-$, $\eta \to \gamma\gamma$) or -0.08 GeV $< \Delta E < 0.06$ GeV for $B^0 \to \eta' K^0_S$ ($\eta' \to \eta\pi^+\pi^-$, $\eta \to \pi^+\pi^-\pi^0$), and 5.27 GeV/c^2 $< M_{\rm bc} <$ 5.29 GeV/c^2 for all decays. The continuum suppression is based on the likelihood ratio $\mathcal{R}_{\rm s/b}$ obtained from the same discriminating variables used for the $B^0 \to \phi K^0_S$ decay, except that $\cos\theta_H$ for B^0 decays is not used; we only use the helicity angle for the decay $\eta' \to \rho\gamma$ ($\rho \to \pi^+\pi^-$), which is defined as the angle between the η' meson momentum and the daughter π^+ momentum in the ρ meson rest frame. The minimum $\mathcal{R}_{\rm s/b}$ requirement depends both on the decay mode and on the flavor-tagging quality, and ranges from 0 (i.e. no requirement) to 0.4.

We use events outside the signal region as well as a large MC sample to study the background components. The dominant background is from continuum. In addition, according to MC simulation, there is a small ($\sim 3\%$) contamination from $B\overline{B}$ background events in

$B^0 \to \eta' K^0_S$ ($\eta' \to \rho^0\gamma$). The contributions from $B\overline{B}$ events are smaller for other modes. The influence of these backgrounds is treated as a source of systematic uncertainty.

Figure 1(e) shows the $M_{\rm bc}$ distribution for the reconstructed $B^0 \to \eta' K^0_S$ candidates within the ΔE values signal region after flavor tagging and vertex reconstruction. The signal yield is determined from unbinned two-dimensional maximum-likelihood fits to the ΔE-$M_{\rm bc}$ distributions in the fit region defined as 5.2 GeV/c^2 $< M_{\rm bc} <$ 5.3 GeV/c^2 and -0.25 GeV $< \Delta E <$ 0.25 GeV. We perform the fit for each final state separately. The $\eta' K^0_S$ signal distribution is modeled with a sum of two (three) Gaussian functions for $M_{\rm bc}$ (ΔE). For the continuum background, we use the ARGUS parameterization for $M_{\rm bc}$ and a linear function for ΔE. For the $\eta' \to \rho\gamma$ mode, we include the $B\overline{B}$ background shape obtained from MC in the fits. The fits yield a total of 512 ± 27 $B^0 \to \eta' K^0_S$ events in the signal region, where the error is statistical only.

F. $B^0 \to \omega K^0_S$

Candidate $K^0_S \to \pi^+\pi^-$ decays are selected with criteria that are identical to those used for the $B^0 \to \phi K^0_S$ decay. Pions for the $\omega \to \pi^+\pi^-\pi^0$ decay are selected with the same criteria used for the $\eta \to \pi^+\pi^-\pi^0$ decay, except that we require $p^{\rm cms}_{\pi^0} > 0.35$ GeV/c. The $\pi^+\pi^-\pi^0$ invariant mass is required to be within 0.03 GeV/c^2 of the nominal ω mass. The B meson signal region is defined as $|\Delta E| < 0.06$ GeV and 5.27 GeV/c^2 $< M_{\rm bc} <$ 5.29 GeV/c^2. The dominant background is from continuum. The continuum suppression is based on the likelihood ratio $\mathcal{R}_{\rm s/b}$ obtained from the same discriminating variables used for the $B^0 \to \phi K^0_S$ decay; the helicity angle θ_H is defined as the angle between the B^0 meson momentum and the cross product of the π^+ and π^- momenta in the ω meson rest frame. The minimum $\mathcal{R}_{\rm s/b}$ requirement depends both on the decay mode and on the flavor-tagging quality, and ranges from 0.3 (used for $r > 0.875$) to 0.9 (used for $r < 0.25$). The contribution from $B\overline{B}$ events is negligibly small.

Figure 1(f) shows the $M_{\rm bc}$ distribution for the reconstructed $B^0 \to \omega K^0_S$ candidates within the ΔE signal region after flavor tagging and vertex reconstruction. The signal yield is determined from an unbinned two-dimensional maximum-likelihood fit to the ΔE-$M_{\rm bc}$ distribution in the fit region defined as 5.2 GeV/c^2 $< M_{\rm bc} <$ 5.3 GeV/c^2 and -0.12 GeV $< \Delta E <$ 0.25 GeV. The ΔE distribution is modeled with a sum of two (three) Gaussian functions for $M_{\rm bc}$ (ΔE). For the continuum background, we use the ARGUS parameterization for $M_{\rm bc}$ and a linear function for ΔE. The fit yields 31 ± 7 $B^0 \to \omega K^0_S$ events in the signal region with a statistical significance (Σ) of 7.3, where Σ is defined as $\Sigma \equiv \sqrt{-2\ln(\mathcal{L}_0/\mathcal{L}_{N_{\rm sig}})}$, and $\mathcal{L}_0$ and $\mathcal{L}_{N_{\rm sig}}$ denote the maximum likelihoods of the fits without and with the signal component, respectively.

G. $B^0 \to K^0_S\pi^0$

Candidate $K^0_S \to \pi^+\pi^-$ decays are selected with the same criteria as those used for the $B^0 \to \phi K^0_S$ decay, except that we impose a more stringent invariant mass requirement; only pairs of oppositely charged pions that have an invariant mass within 0.015 GeV/c^2 of the nominal K^0_S mass are used. The π^0 selection criteria are the same as those used for the $B^0 \to \eta' K^0_S$ decay.

The B meson signal region is defined as -0.15 GeV $< \Delta E < 0.1$ GeV and 5.27 GeV/c^2 $< M_{\rm bc} <$ 5.29 GeV/c^2. The dominant background is from continuum. We use extended modified Fox-Wolfram moments, which were applied for the selection of the $B^0 \to \pi^0\pi^0$ decay [20], to form $\mathcal{F}$. We then combine likelihoods for $\mathcal{F}$ and $\cos\theta_B$ to obtain the event likelihood ratio $\mathcal{R}_{\rm s/b}$ for continuum suppression. As described below, we include events that do not have B decay vertex information in our fit to obtain a better sensitivity for the CP-violation parameter $\mathcal{A}$. For events with vertex information, the high-$\mathcal{R}_{\rm s/b}$ region is defined as $\mathcal{R}_{\rm s/b} > 0.74$ (0.76) for DS-I (DS-II), and the low-$\mathcal{R}_{\rm s/b}$ region as $0.4 < \mathcal{R}_{\rm s/b} \leq 0.74$ (0.76) for DS-I (DS-II). For events without vertex information, the high-$\mathcal{R}_{\rm s/b}$ region is defined as $\mathcal{R}_{\rm s/b} > 0.78$ and the low-$\mathcal{R}_{\rm s/b}$ region as $0.4 < \mathcal{R}_{\rm s/b} \leq 0.78$ for both DS-I and DS-II.

Figure 1(g) shows the $M_{\rm bc}$ distribution for the high-$\mathcal{R}_{\rm s/b}$ $B^0 \to K^0_S\pi^0$ candidates within the ΔE signal region after flavor tagging and before vertex reconstruction. Also shown in Fig. 1(h) is the $M_{\rm bc}$ distribution for the low-$\mathcal{R}_{\rm s/b}$ $B^0 \to K^0_S\pi^0$ candidates. The signal yield is determined from an unbinned two-dimensional maximum-likelihood fit to the ΔE-$M_{\rm bc}$ distribution in the fit region defined as 5.2 GeV/c^2 $< M_{\rm bc} <$ 5.29 GeV/c^2 and -0.2 GeV $< \Delta E <$ 0.5 GeV. The $B^0 \to K^0_S\pi^0$ signal distribution is modeled with a Gaussian function for $M_{\rm bc}$ and with a Crystal Ball function for ΔE. For the continuum background, we use the ARGUS parameterization for $M_{\rm bc}$ and a second-order Chebyshev function for ΔE. The $B\overline{B}$ background is negligibly small and its influence is treated as a source of systematic uncertainty. The fits yield 168 ± 16 and 83 ± 18 $B^0 \to K^0_S\pi^0$ events in the high-$\mathcal{R}_{\rm s/b}$ and low-$\mathcal{R}_{\rm s/b}$ signal regions, respectively, where the errors are statistical only. The same procedure after the vertex reconstruction yields a total of 77 ± 13 $K^0_S\pi^0$ events.

H. $B^0 \to K^{*0}\gamma$ ($K^{*0} \to K^0_S\pi^0$)

The selection criteria are optimized for the measurement of time-dependent CP asymmetries and are thus different from those used in Belle's previous measurement of $B \to K^*\gamma$ branching fractions and direct CP asymmetries [21]. Candidate $K^0_S \to \pi^+\pi^-$ decays are selected with the same criteria as those used for the $B^0 \to \phi K^0_S$ decay, except that we impose a more stringent invariant mass requirement; only pairs of oppositely charged pions that have an invariant mass within 0.006 GeV/c^2 of the nominal K^0_S mass are used. The π^0 selection criteria are the same as those used for the $B^0 \to \eta' K^0_S$ decay except for a more stringent π^0 momentum requirement, $p^{\rm cms}_{\pi^0} > 0.3$ GeV/c. The $K^0_S\pi^0$ invariant mass, $M_{K^0_S\pi^0}$, is required to be between 0.6 and 1.8 GeV/c^2.

Prompt photons from the $B^0 \to K^{*0}\gamma$ decay are required to satisfy 1.4 GeV $< E^{\rm cms}_\gamma <$ 3.4 GeV, where $E^{\rm cms}_\gamma$ is the photon energy in the cms. If there is more than one candidate, the one with the largest $E^{\rm cms}_\gamma$ is selected. For the selected photon, we require $E_9/E_{25} > 0.95$, where E_9/E_{25} is defined in Sec. II C. Photons for candidate $\pi^0 \to \gamma\gamma$ or $\eta \to \gamma\gamma$ decays are not used; we reject photon pairs that satisfy $\mathcal{L}_{\pi^0} \geq 0.18$ or $\mathcal{L}_\eta \geq 0.18$, where $\mathcal{L}_{\pi^0(\eta)}$ is a π^0 (η) likelihood described in detail elsewhere [22]. The polar angle of the photon direction in the laboratory frame is required to be between 33° and 128° for DS-I, while no requirement is imposed for DS-II as the material within the acceptance of the ECL is much reduced for this dataset.

Candidate $K^{*+} \to K^0_S\pi^+$ decays are also selected using a similar procedure to reconstruct the decay $B^0 \to K^{*+}\gamma$. Candidate $B^0 \to K^{*0}\gamma$ ($K^{*0} \to K^0_S\pi^0$) and $B^+ \to K^{*+}\gamma$ ($K^{*+} \to K^0_S\pi^+$) decays are selected simultaneously; we allow only one candidate for each event. The best candidate selection is based on the event likelihood ratio $\mathcal{R}_{\rm s/b}$ that is obtained by

combining $\mathcal{F}$, which uses the extended modified Fox-Wolfram moments as discriminating variables, with $\cos\theta_H$ defined as the angle between the B^0 meson momentum and the daughter K^0_S momentum in the K^{*0} meson rest frame. We select the candidate with the largest $\mathcal{R}_{\rm s/b}$.

The signal region for the $B^0 \to K^{*0}\gamma$ ($K^{*0} \to K^0_S\pi^0$) decay is defined as -0.2 GeV $< \Delta E < 0.1$ GeV, 5.27 GeV/$c^2 < M_{\rm bc} < 5.29$ GeV/c^2 and 0.8GeV/$c^2 < M_{K^0_S\pi^0} < 1.0$ GeV/c^2. We require $\mathcal{R}_{\rm s/b} > 0.5$ to reduce the continuum background.

We use events outside the signal region as well as a large MC sample to study the background components. The dominant background is from continuum. Background contributions from B decays are significantly smaller than those from continuum, and are dominated by cross-feed from $B^+ \to K^{*+}\gamma$ decays, other radiative B decays and charmless B decays. Background from other $B\overline{B}$ decays is found to be negligible.

Figure 1(i) shows the $M_{\rm bc}$ distribution for the reconstructed $B^0 \to K^{*0}\gamma$ candidates within the ΔE signal region after flavor tagging and vertex reconstruction. The signal yield is determined from an unbinned two-dimensional maximum-likelihood fit to the ΔE-$M_{\rm bc}$ distribution in the fit region defined as 5.20 GeV/$c^2 < M_{\rm bc} < 5.29$ GeV/c^2 and -0.5 GeV $< \Delta E < 0.5$ GeV. The $B^0 \to K^{*0}\gamma$ signal distribution is represented by a smoothed histogram obtained from MC simulation that accounts for the correlation between $M_{\rm bc}$ and ΔE. The background from B decays is also modeled with a smoothed histogram obtained from MC events; its normalization is a free parameter in the fit. For the continuum background, we use the ARGUS parameterization for $M_{\rm bc}$ and a second-order Chebyshev function for ΔE. The fit yields 57 ± 9 $B^0 \to K^{*0}\gamma$ ($K^{*0} \to K^0_S\pi^0$) events, where the error is statistical only. For reference, we also measure the signal before vertex reconstruction and obtain 132 ± 14 events.

I. Flavor Tagging

The b-flavor of the accompanying B meson is identified from inclusive properties of particles that are not associated with the reconstructed $B^0 \to f_{CP}$ decay. We use the same procedure that is used for the $\sin 2\phi_1$ measurement [10]. The algorithm for flavor tagging is described in detail elsewhere [23]. We use two parameters, q and r, to represent the tagging information. The first, q, is already defined in Eq. (1). The parameter r is an event-by-event, MC-determined flavor-tagging dilution factor that ranges from $r = 0$ for no flavor discrimination to $r = 1$ for unambiguous flavor assignment. It is used only to sort data into six r intervals. The wrong tag fractions for the six r intervals, w_l ($l = 1, 6$), and differences between B^0 and $\overline{B}^0$ decays, Δw_l, are determined from the data; we use the same values that were used for the $\sin 2\phi_1$ measurement [10] for DS-I. Wrong tag fractions for DS-II are separately obtained with the same procedure; we find that the values for DS-II, which are listed in Table I, are slightly smaller than those for DS-I. The total effective tagging efficiency for DS-II is determined to be $\epsilon_{\rm eff} \equiv \sum_{l=1}^{6} \epsilon_l (1 - 2w_l)^2 = 0.30 \pm 0.01$, where ϵ_l is the event fraction for each r interval determined from the $J/\psi K^0_S$ data and listed in Table I. The error includes both statistical and systematic uncertainties.

J. Vertex Reconstruction

The vertex position for the f_{CP} decay is reconstructed using charged tracks that have enough SVD hits. A constraint on the IP is also used with the selected tracks; the IP profile is convolved with finite B flight length in the plane perpendicular to the z axis. The pions from K^0_S decays are not used except for the analysis of $B^0 \to K^{*0}\gamma$ and $B^0 \to K^0_S\pi^0$ decays. The vertex for $B^0 \to K^{*0}\gamma$ and $B^0 \to K^0_S\pi^0$ decays is reconstructed using the K^0_S trajectory and the IP constraint, where both pions from the K^0_S decay are required to have enough SVD hits to reconstruct a vertex. The reconstruction efficiency depends both on the K^0_S momentum and on the SVD geometry; efficiencies with SVD-II are higher than those with SVD-I because of the larger outer radius and the additional layer.

The $f_{\rm tag}$ vertex determination with SVD-I remains unchanged from the previous publication [4], and is described in detail elsewhere [24]; to minimize the effect of long-lived particles, secondary vertices from charmed hadrons and a small fraction of poorly reconstructed tracks, we adopt an iterative procedure in which the track that gives the largest contribution to the vertex χ^2 is removed at each step until a good χ^2 is obtained.

For SVD-II, we find that the same vertex reconstruction algorithm results in a larger outlier fraction when only one track remains after the iteration procedure. Therefore, in this case, we repeat the iteration procedure with a more stringent requirement on the SVD-II hit pattern. The resulting outlier fraction is comparable to that for SVD-I, while the inefficiency caused by this change is small (2.5%).

K. Summary of Signal Yields

The signal yields for $B^0 \to f_{CP}$ decays, $N_{\rm sig}$, after flavor tagging and vertex reconstruction (before the vertex reconstruction for the decay $B^0 \to K^0_S\pi^0$) are summarized in Table II. The signal purities are also listed in the table.

III. RESULTS OF CP ASYMMETRY MEASUREMENTS

We determine $\mathcal{S}$ and $\mathcal{A}$ for each mode by performing an unbinned maximum-likelihood fit to the observed Δt distribution. The probability density function (PDF) expected for the signal distribution, $\mathcal{P}_{\rm sig}(\Delta t; \mathcal{S}, \mathcal{A}, q, w_l, \Delta w_l)$, is given by Eq. (1) incorporating the effect of incorrect flavor assignment. The distribution is convolved with the proper-time interval resolution function $R_{\rm sig}(\Delta t)$, which takes into account the finite vertex resolution.

For the decays $B^0 \to \phi K^0_S$, $K^+K^-K^0_S$, ϕK^0_L, $f_0(980)K^0_S$, $\eta' K^0_S$ and ωK^0_S, we use flavor-specific B decays governed by semileptonic or hadronic $b \to c$ transitions to determine the resolution function. We perform a simultaneous multi-parameter fit to these high-statistics control samples to obtain the resolution function parameters, wrong-tag fractions (Section II I), Δm_d, τ_{B^+} and τ_{B^0}. We use the same resolution function used for the $\sin 2\phi_1$ measurement for DS-I [10]. For DS-II, the following modifications are introduced: a sum of two Gaussian functions is used to model the resolution of the f_{CP} vertex while a single Gaussian function is used for DS-I; a sum of two Gaussian functions is used to model the resolution of the tag-side vertex obtained with one track and the IP constraint, while a single Gaussian function is used for DS-I. These modifications are needed to account for differences for SVD-I and SVD-II, as well as different background conditions in DS-I and

DS-II. We test the new resolution parameterization using MC events on which we overlay beam-related background taken from data. A fit to the MC sample yields correct values for all parameters. With the multi-parameter fit to data, we find that the standard deviation of the main Gaussian component of the resolution function is reduced from 78 μm to 55 μm, which is consistent with our expectation from the improved impact parameter resolution of SVD-II [16]. The same fit also yields $\tau_{B^0} = 1.518 \pm 0.012$ ps, $\tau_{B^+} = 1.652 \pm 0.014$ ps and $\Delta m_d = 0.516 \pm 0.007$ ps^{-1}. The results are consistent with those obtained with DS-I [10] and also with the world average values [26]. Thus we conclude that the resolution of SVD-II is well understood.

For the decays $B^0 \to K^0_S\pi^0$ and $K^{*0}\gamma$ ($K^{*0} \to K^0_S\pi^0$), we use the resolution function described above with additional parameters that rescale vertex errors. The rescaling parameters depend on the detector configuration (SVD-I or SVD-II), SVD hit patterns of charged pions from the K^0_S decay, and K^0_S decay vertex position in the plane perpendicular to the beam axis. These parameters are determined from a fit to the Δt distribution of $B^0 \to J/\psi K^0_S$ data. Here the K^0_S and the IP constraint are used for the vertex reconstruction, the B^0 lifetime is fixed at the world average value, and b-flavor tagging information is not used so that the expected PDF is an exponential function convolved with the resolution function.

We check the resulting resolution function by also reconstructing the vertex with leptons from J/ψ decays and the IP constraint. We find that the distribution of the distance between the vertex positions obtained with the two methods is well represented by the obtained resolution function convolved with the well-known resolution for the J/ψ vertex. Finally, we also perform a fit to the $B^0 \to J/\psi K^0_S$ sample with b-flavor information and obtain $\mathcal{S}_{J/\psi K^0_S} = +0.68 \pm 0.10$(stat) and $\mathcal{A}_{J/\psi K^0_S} = +0.02 \pm 0.04$(stat), which are in good agreement with the world average values. Thus, we conclude that the vertex resolution for the $B^0 \to K^0_S\pi^0$ and $B^0 \to K^{*0}\gamma$ ($K^{*0} \to K^0_S\pi^0$) decays is well understood.

We determine the following likelihood value for each event:

$$\begin{aligned} P_i \;=\; & (1 - f_{\rm ol}) \int \Big[f_{\rm sig}\mathcal{P}_{\rm sig}(\Delta t') R_{\rm sig}(\Delta t_i - \Delta t') \\ & +\; (1 - f_{\rm sig})\mathcal{P}_{\rm bkg}(\Delta t') R_{\rm bkg}(\Delta t_i - \Delta t') \Big] d(\Delta t') \\ & +\; f_{\rm ol} P_{\rm ol}(\Delta t_i) \end{aligned} \qquad (2)$$

where $P_{\rm ol}(\Delta t)$ is a broad Gaussian function that represents an outlier component with a small fraction $f_{\rm ol}$. The signal probability $f_{\rm sig}$ depends on the r region and is calculated on an event-by-event basis as a function of $p_B^{\rm cms}$ for the $B^0 \to \phi K^0_L$ decay and as a function of ΔE and $M_{\rm bc}$ for the other modes. A PDF for background events, $\mathcal{P}_{\rm bkg}(\Delta t)$, is modeled as a sum of exponential and prompt components, and is convolved with a sum of two Gaussians $R_{\rm bkg}$. All parameters in $\mathcal{P}_{\rm bkg}(\Delta t)$ and $R_{\rm bkg}$ are determined by the fit to the Δt distribution of a background-enhanced control sample [25]; i.e. events outside of the ΔE-$M_{\rm bc}$ signal region. We fix τ_{B^0} and Δm_d at their world-average values [26]. In order to reduce the statistical error on $\mathcal{A}$, we include events without vertex information in the analysis of $B^0 \to K^0_S\pi^0$. The likelihood value in this case is obtained by integrating Eq. (2) over Δt_i.

The only free parameters in the final fit are $\mathcal{S}$ and $\mathcal{A}$, which are determined by maximizing the likelihood function $L = \prod_i P_i(\Delta t_i; \mathcal{S}, \mathcal{A})$ where the product is over all events. Since $\mathcal{A}$ for the decay $B^0 \to K^{*0}\gamma$ is well measured in the $B^0 \to K^{*0}\gamma$ ($K^{*0} \to K^+\pi^-$) mode and is consistent with zero, we fix $\mathcal{A}$ at zero and perform a fit to the $B^0 \to K^{*0}\gamma$ ($K^{*0} \to K^0_S\pi^0$) sample with $\mathcal{S}$ as the only free parameter.

Table III summarizes the fit results of $\mathcal{S}$ and $\mathcal{A}$. We define the raw asymmetry in each Δt bin by $(N_{q=+1} - N_{q=-1})/(N_{q=+1} + N_{q=-1})$, where $N_{q=+1(-1)}$ is the number of observed candidates with $q = +1(-1)$ [27]. Figures 2(a-g) show the raw asymmetries in two regions of the flavor-tagging parameter r. While the numbers of events in the two regions are similar, the effective tagging efficiency is much larger and the background dilution is smaller in the region $0.5 < r \leq 1.0$. Note that these projections onto the Δt axis do not take into account event-by-event information (such as the signal fraction, the wrong tag fraction and the vertex resolution), which is used in the unbinned maximum-likelihood fit.

Tables IV and V list the systematic errors on $\mathcal{S}$ and $\mathcal{A}$, respectively. The total systematic errors are obtained by adding each contribution in quadrature, and are much smaller than the statistical errors for all modes.

To determine the systematic error that arises from uncertainties in the vertex reconstruction, the track and vertex selection criteria are varied to search for possible systematic biases. Small biases in the Δz measurement are observed in $e^+e^- \to \mu^+\mu^-$ and other control samples. Systematic errors are estimated by applying special correction functions to account for the observed biases, repeating the fit, and comparing the obtained values with the nominal results. The systematic error due to the IP constraint in the vertex reconstruction is estimated by varying ($\pm 10\mu$m) the smearing used to account for the B flight length. Systematic errors due to imperfect SVD alignment are determined from MC samples that have artificial mis-alignment effects to reproduce impact-parameter resolutions observed in data.

Systematic errors due to uncertainties in the wrong tag fractions are studied by varying the wrong tag fraction individually for each r region. Systematic errors due to uncertainties in the resolution function are also estimated by varying each resolution parameter obtained from data (MC) by $\pm 1\sigma$ ($\pm 2\sigma$), repeating the fit and adding each variation in quadrature. Each physics parameter such as τ_{B^0} and Δm_d is also varied by its error. A possible fit bias is examined by fitting a large number of MC events.

Systematic errors from uncertainties in the background fractions and in the background Δt shape are estimated by varying each background parameter obtained from data (MC) by $\pm 1\sigma$ ($\pm 2\sigma$). Uncertainties in the background B decay model are also considered for the $B^0 \to K^{*0}\gamma$ ($K^{*0} \to K^0_S\pi^0$) mode; we compare different theoretical models for radiative B decays and take the largest variation as the systematic error.

Additional sources of systematic errors are considered for B decay backgrounds that are neglected in the PDF. We consider uncertainties both in their fractions and CP asymmetries; for modes that have non-vanishing CP asymmetries, we conservatively vary the CP-violation parameters within the physical region and take the largest variation as the systematic error. The effect of backgrounds from $K^+K^-K^0_S$ and $f_0(980)K^0_S$ ($f_0(980) \to K^+K^-$) in the $B^0 \to \phi K^0_S$ sample is considered. Uncertainties from $B \to \phi K^*$ and other rare B decay backgrounds in the $B^0 \to \phi K^0_L$ sample are also taken into account. The peaking background fraction in the $B^0 \to f_0(980)K^0_S$ sample depends on the PDF used in the fit to the $\pi^+\pi^-$ invariant mass distribution, which ignores possible interference between resonant and non-resonant amplitudes. We perform a fit to the $\pi^+\pi^-$ distribution of a MC sample generated with interfering amplitudes and phases for $B \to K\pi\pi$ decays measured from data [19]. The observed difference in the signal yield from the true value is taken into account in the systematic error determination. We also repeat the fit to the Δt distribution ignoring the contribution of the peaking background. The differences in $\mathcal{S}$ and $\mathcal{A}$ from our nominal results are included in the systematic error.

Finally, we investigate the effects of interference between CKM-favored and CKM-suppressed $B \to D$ transitions in the $f_{\rm tag}$ final state [28]. A small correction to the PDF for the signal distribution arises from the interference. We estimate the size of the correction using the $B^0 \to D^{*-}\ell^+\nu$ sample. We then generate MC pseudo-experiments and make an ensemble test to obtain systematic biases in $\mathcal{S}$ and $\mathcal{A}$. We find that the effect on $\mathcal{S}$ is negligibly small, while a possible shift in $\mathcal{A}$ is sizable.

Various crosschecks of the measurement are performed. We reconstruct charged B meson decays that are the counterparts of the $B^0 \to f_{CP}$ decays and apply the same fit procedure. All results for the $\mathcal{S}$ term are consistent with no CP asymmetry, as expected. Lifetime measurements are also performed for the f_{CP} modes and the corresponding charged B decay modes. The fits yield τ_{B^0} and τ_{B^+} values consistent with the world-average values. MC pseudo-experiments are generated for each decay mode to perform ensemble tests. We find that the statistical errors obtained in our measurements are all consistent with the expectations from the ensemble tests.

For the $B^0 \to \phi K^0$ decay, a fit to DS-I alone yields $\mathcal{S} = -0.68 \pm 0.46$(stat) and $\mathcal{A} = -0.02 \pm 0.28$(stat), while a fit to DS-II alone yields $\mathcal{S} = +0.78 \pm 0.45$(stat) and $\mathcal{A} = +0.17 \pm 0.33$(stat). Note that the results for DS-I differ from our previously published results $\mathcal{S} = -0.96 \pm 0.50^{+0.09}_{-0.11}$ and $\mathcal{A} = -0.15 \pm 0.29 \pm 0.07$ [4], as decays $B^0 \to \phi K^0_L$ and ϕK^0_S ($K^0_S \to \pi^0\pi^0$) are included in this analysis. From MC pseudo-experiments, the probability that the difference between $\mathcal{S}$ values in DS-I and DS-II is larger than the observed difference (1.46) is estimated to be 4.5%. A $\sin 2\phi_1$ measurement with DS-II is performed using $B^0 \to J/\psi K^0_S$ ($K^0_S \to \pi^+\pi^-$ or $\pi^0\pi^0$) and $B^0 \to J/\psi K^0_L$ decays as a crosscheck. Applying the same procedure to both DS-I and DS-II, we obtain $\mathcal{S}_{J/\psi K^0} = +0.696 \pm 0.061$(stat) and $\mathcal{A}_{J/\psi K^0} = +0.011 \pm 0.043$(stat) for DS-I, and $\mathcal{S}_{J/\psi K^0} = +0.629 \pm 0.069$(stat) and $\mathcal{A}_{J/\psi K^0} = +0.035 \pm 0.044$(stat) for DS-II. The results are in good agreement with each other, and are also consistent with SM expectations. As all the other checks mentioned above also yield results consistent with expectations, we conclude that the difference in $\mathcal{S}_{\phi K^0}$ between the two datasets is due to a statistical fluctuation.

A fit to the $B^0 \to K^{*0}\gamma$ ($K^{*0} \to K^0_S\pi^0$) sample with both $\mathcal{A}$ and $\mathcal{S}$ as free parameters yields $\mathcal{S} = -0.79^{+0.63}_{-0.50}$(stat), which is identical with the result of the one parameter fit, and $\mathcal{A} = -0.00 \pm 0.38$(stat), which is consistent with zero.

As discussed in Section I, to a good approximation, the SM predicts $\mathcal{S} = -\xi_f \sin 2\phi_1$ for the $B^0 \to \phi K^0$, $K^+K^-K^0_S$, $f_0(980)K^0_S$, $\eta' K^0_S$, ωK^0_S and $K^0_S\pi^0$ decays. Figure 3 summarizes the $\sin 2\phi_1$ determination based on our $\mathcal{S}$ measurements for these decays. For each mode, the first error shown in the figure is statistical and the second error is systematic. For the $B^0 \to K^+K^-K^0_S$ decay, an additional systematic error that arises from the uncertainty of the CP-even component fraction ($^{+0.17}_{-0.00}$) is added in quadrature. We obtain $\sin 2\phi_1 = +0.43^{+0.12}_{-0.11}$ as a weighted average, where the error includes both statistical and systematic errors. The result differs from the SM expectation by 2.4 standard deviations.

IV. SUMMARY

We have performed improved measurements of CP-violation parameters for $B^0 \to \phi K^0$ (including both ϕK^0_S and ϕK^0_L), $K^+K^-K^0_S$ and $\eta' K^0_S$ decays, and new measurements for $B^0 \to f_0(980)K^0_S$, ωK^0_S and $K^0_S\pi^0$ decays. These charmless decays are dominated by $b \to s$ flavor-changing neutral currents and are sensitive to possible new CP-violating phases. We have also measured the time-dependent CP asymmetry in the decay $K^{*0}\gamma$ ($K^{*0} \to K^0_S\pi^0$),

which is also sensitive to physics beyond the SM. The results for each individual decay mode are consistent with the SM expectation within two standard deviations except for the $B^0 \to f_0(980)K^0_S$ decay. The combined result for the $B^0 \to \phi K^0$, $K^+K^-K^0_S$, $f_0(980)K^0_S$, $\eta' K^0_S$, ωK^0_S and $K^0_S\pi^0$ decays differs from the SM expectation by 2.4 standard deviations. Measurements with a much larger data sample are required to conclusively establish the existence of a new CP-violating phase beyond the SM.

Acknowledgments

We thank the KEKB group for the excellent operation of the accelerator, the KEK Cryogenics group for the efficient operation of the solenoid, and the KEK computer group and the National Institute of Informatics for valuable computing and Super-SINET network support. We acknowledge support from the Ministry of Education, Culture, Sports, Science, and Technology of Japan and the Japan Society for the Promotion of Science; the Australian Research Council and the Australian Department of Education, Science and Training; the National Science Foundation of China under contract No. 10175071; the Department of Science and Technology of India; the BK21 program of the Ministry of Education of Korea and the CHEP SRC program of the Korea Science and Engineering Foundation; the Polish State Committee for Scientific Research under contract No. 2P03B 01324; the Ministry of Science and Technology of the Russian Federation; the Ministry of Education, Science and Sport of the Republic of Slovenia; the National Science Council and the Ministry of Education of Taiwan; and the U.S. Department of Energy.

---

[1] A. G. Akeroyd *et al.*, hep-ex/0406071 and references therein.
[2] See for example,
Y. Grossman and M. P. Worah, Phys. Lett. B **395**, 241 (1997); T. Moroi, Phys. Lett. B **493**, 366 (2000); D. Chang, A. Masiero and H. Murayama, Phys. Rev. D **67**, 075013 (2003); S. Baek, T. Goto, Y. Okada and K. i. Okumura, Phys. Rev. D **64**, 095001 (2001).
[3] Throughout this paper, the inclusion of the charge conjugate decay mode is implied unless otherwise stated.
[4] Belle Collaboration, K. Abe *et al.*, Phys. Rev. Lett. **91**, 261602 (2003).
[5] BaBar Collaboration, B. Aubert *et al.*, hep-ex/0408062; hep-ex/0408072; hep-ex/0408076; hep-ex/0408090; hep-ex/0408095.
[6] Heavy Flavor Averaging Group, http://www.slac.stanford.edu/xorg/hfag/.
[7] M. Kobayashi and T. Maskawa, Prog. Theor. Phys. **49**, 652 (1973).
[8] A. B. Carter and A. I. Sanda, Phys. Rev. D **23**, 1567 (1981); I. I. Bigi and A. I. Sanda, Nucl. Phys. **B193**, 85 (1981).
[9] Belle Collaboration, K. Abe *et al.*, Phys. Rev. Lett. **87**, 091802 (2001); Phys. Rev. D **66**, 032007 (2002); Phys. Rev. D **66**, 071102 (2002).
[10] Belle Collaboration, K. Abe *et al.*, BELLE-CONF-0436, hep-ex/0408036.
[11] BaBar Collaboration, B. Aubert *et al.*, Phys. Rev. Lett. **89**, 201802 (2002).
[12] BaBar Collaboration, B. Aubert *et al.*, hep-ex/0405082.
[13] D. Atwood, M. Gronau and A. Soni, Phys. Rev. Lett. **79**, 185 (1997).
[14] S. Kurokawa and E. Kikutani *et al.*, Nucl. Instr. and Meth. A **499**, 1 (2003).

[15] Belle Collaboration, A. Abashian *et al.*, Nucl. Instr. and Meth. A **479**, 117 (2002).
[16] Y. Ushiroda (Belle SVD2 Group), Nucl. Instr. and Meth. A **511**, 6 (2003).
[17] Belle Collaboration, K. Abe *et al.*, Phys. Rev. Lett. **87**, 101801 (2001).
[18] ARGUS Collaboration, H. Albrecht *et al.*, Phys. Lett. B **241**, 278 (1990).
[19] Belle Collaboration, A. Garmash *et al.*, Phys. Rev. D **69**, 012001 (2004); Belle Collaboration, K. Abe *et al.*, Belle-CONF-0410 (2004).
[20] Belle Collaboration, K. Abe *et al.*, Phys. Rev. Lett. **91**, 261801 (2003).
[21] Belle Collaboration, M. Nakao *et al.*, Phys. Rev. D **69**, 112001 (2004).
[22] Belle Collaboration, P. Koppenburg *et al.*, Phys. Rev. Lett. **93**, 061803 (2004).
[23] H. Kakuno, K. Hara *et al.*, hep-ex/0403022, to appear in Nucl. Instr. and Meth. A.
[24] H. Tajima *et al.*, hep-ex/0301026, to appear in Nucl. Instr. and Meth. A.
[25] Parameters in $\mathcal{P}_{\rm bkg}(\Delta t)$ and $R_{\rm bkg}$ for $B\overline{B}$ background events in $B^0 \to \eta' K^0_S$ decay are determined from MC simulation.
[26] S. Eidelman *et al.*, Phys. Lett. B **592**, 1 (2004).
[27] We use an alternative definition of the raw asymmetry, $(N_{q\xi_f=-1} - N_{q\xi_f=+1})/(N_{q\xi_f=-1} + N_{q\xi_f=+1})$, for the decay $B^0 \to \phi K^0$ to take the opposite CP parities for the decays $B^0 \to \phi K^0_S$ and ϕK^0_L into account.
[28] O. Long, M. Baak, R. N. Cahn and D. Kirkby, Phys. Rev. D **68**, 034010 (2003).

TABLE I: The event fractions ϵ_l, wrong-tag fractions w_l, wrong-tag fraction differences Δw_l, and average effective tagging efficiencies $\epsilon^l_{\rm eff} = \epsilon_l(1-2w_l)^2$ for each r interval for the DS-II. The errors for w_l and Δw_l include both statistical and systematic uncertainties. The event fractions are obtained from $J/\psi K^0_S$ data.

l	r interval	ϵ_l	w_l	Δw_l	$\epsilon^l_{\rm eff}$
1	0.000 – 0.250	0.397 ± 0.015	0.464 ± 0.007	$+0.010 \pm 0.007$	0.002 ± 0.001
2	0.250 – 0.500	0.146 ± 0.009	0.321 ± 0.008	-0.022 ± 0.010	0.019 ± 0.002
3	0.500 – 0.625	0.108 ± 0.008	0.224 ± 0.011	$+0.031 \pm 0.011$	0.033 ± 0.004
4	0.625 – 0.750	0.107 ± 0.008	0.157 ± 0.010	$+0.002 \pm 0.011$	0.051 ± 0.005
5	0.750 – 0.875	0.098 ± 0.007	0.109 ± 0.009	-0.028 ± 0.011	0.060 ± 0.005
6	0.875 – 1.000	0.144 ± 0.009	0.016 ± 0.005	$+0.007 \pm 0.007$	0.135 ± 0.009

TABLE II: The estimated signal purity and the signal yield $N_{\rm sig}$ in the signal region for each f_{CP} mode that is used to measure CP asymmetries. The result for the $B^0 \to K^0_S\pi^0$ decay is obtained with the sample after flavor tagging but before vertex reconstruction as events that do not have vertex information are also used to extract the direct CP violation parameter $\mathcal{A}$. The results for the other decays are obtained after flavor tagging and vertex reconstruction.

Mode		ξ_f	purity	$N_{\rm sig}$
ϕK^0_S		-1	0.63	139 ± 14
ϕK^0_L		$+1$	0.17	36 ± 15
$K^+K^-K^0_S$		$+1$	0.56	399 ± 28
$f_0(980)K^0_S$		$+1$	0.53	94 ± 14
$\eta' K^0_S$		-1	0.61	512 ± 27
ωK^0_S		-1	0.56	31 ± 7
$K^0_S\pi^0$	(high-$\mathcal{R}_{\rm s/b}$)	-1	0.55	168 ± 16
	(low-$\mathcal{R}_{\rm s/b}$)	-1	0.17	83 ± 18
$K^{*0}(K^0_S\pi^0)\gamma$			0.65	57 ± 9

TABLE III: Results of the fits to the Δt distributions. The first error is statistical and the second error is systematic. We combine $B^0 \to \phi K^0_S$ and $B^0 \to \phi K^0_L$ decays to obtain $\mathcal{S}_{\phi K^0}$ and $\mathcal{A}_{\phi K^0}$.

Mode	SM expectation for $\mathcal{S}$	$\mathcal{S}$	$\mathcal{A}$
ϕK^0	$+\sin 2\phi_1$	$+0.06 \pm 0.33 \pm 0.09$	$+0.08 \pm 0.22 \pm 0.09$
$K^+K^-K^0_S$	$-\sin 2\phi_1$	$-0.49 \pm 0.18 \pm 0.04$	$-0.08 \pm 0.12 \pm 0.07$
$f_0(980)K^0_S$	$-\sin 2\phi_1$	$+0.47 \pm 0.41 \pm 0.08$	$-0.39 \pm 0.27 \pm 0.08$
$\eta' K^0_S$	$+\sin 2\phi_1$	$+0.65 \pm 0.18 \pm 0.04$	$-0.19 \pm 0.11 \pm 0.05$
ωK^0_S	$+\sin 2\phi_1$	$+0.75 \pm 0.64^{+0.13}_{-0.16}$	$+0.26 \pm 0.48 \pm 0.15$
$K^0_S\pi^0$	$+\sin 2\phi_1$	$+0.30 \pm 0.59 \pm 0.11$	$-0.12 \pm 0.20 \pm 0.07$
$K^{*0}\gamma$ ($K^{*0} \to K^0_S\pi^0$)	$-2(m_s/m_b)\sin 2\phi_1$	$-0.79^{+0.63}_{-0.50} \pm 0.10$	-

TABLE IV: Summary of the systematic errors on $\mathcal{S}$.

	ϕK^0	$K^+K^-K^0_S$	$f_0(980)K^0_S$	$\eta' K^0_S$	ωK^0_S	$K^{*0}\gamma$	$K^0_S\pi^0$
Vertex reconstruction	0.01	0.01	0.02	0.01	0.01	0.06	0.02
Flavor tagging	0.01	< 0.01	0.01	0.01	0.04	0.02	0.01
Resolution function	0.04	0.03	0.03	0.03	0.07	0.05	0.05
Physics parameter	< 0.01	< 0.01	0.01	< 0.01	0.01	0.01	0.02
Possible fit bias	0.01	0.01	0.03	0.01	$^{+0.01}_{-0.10}$	0.03	0.03
Background fraction	$^{+0.08}_{-0.06}$	0.02	0.05	0.02	0.10	0.02	0.07
Background Δt shape	0.01	< 0.01	0.04	< 0.01	0.02	0.03	0.04
Tag-side interference	< 0.01	< 0.01	< 0.01	< 0.01	0.01	< 0.01	< 0.01
Total	0.09	0.04	0.08	0.04	$^{+0.13}_{-0.16}$	0.10	0.11

TABLE V: Summary of the systematic errors on $\mathcal{A}$.

	ϕK^0	$K^+K^-K^0_S$	$f_0(980)K^0_S$	$\eta' K^0_S$	ωK^0_S	$K^0_S\pi^0$
Vertex reconstruction	0.03	0.04	0.04	0.03	0.04	0.04
Flavor tagging	< 0.01	< 0.01	0.01	0.01	< 0.01	0.01
Resolution function	0.02	0.02	0.02	0.01	0.04	< 0.01
Physics parameter	< 0.01	< 0.01	< 0.01	< 0.01	< 0.01	< 0.01
Possible fit bias	0.01	0.01	0.03	0.01	$^{+0.01}_{-0.03}$	0.01
Background fraction	0.04	0.01	0.06	0.02	0.14	0.02
Background Δt shape	0.03	< 0.01	0.01	< 0.01	0.03	0.01
Tag-side interference	0.06	0.06	0.03	0.03	0.03	0.05
Total	0.09	0.07	0.08	0.05	0.15	0.07

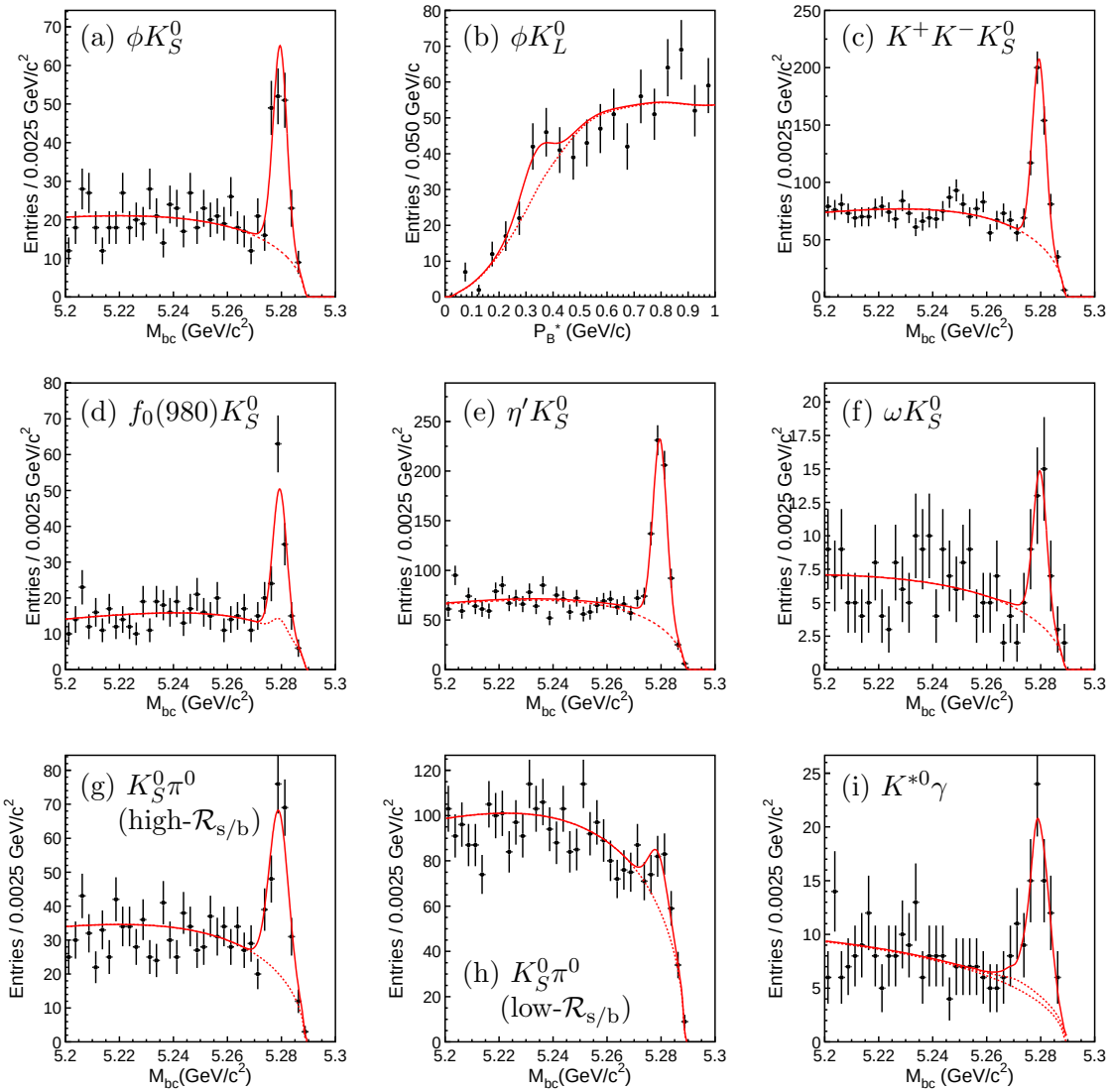

FIG. 1: The $M_{\rm bc}$ distributions for (a) $B^0 \to \phi K^0_S$, (c) $B^0 \to K^+K^-K^0_S$, (d) $B^0 \to f_0(980)K^0_S$, (e) $B^0 \to \eta' K^0_S$, (f) $B^0 \to \omega K^0_S$, (g) $B^0 \to K^0_S\pi^0$ (high-$\mathcal{R}_{\rm s/b}$), (h) $B^0 \to K^0_S\pi^0$ (low-$\mathcal{R}_{\rm s/b}$), and (i) $B^0 \to K^{*0}\gamma$ within the ΔE signal region and (b) the $p^{\rm cms}_B$ distribution for $B^0 \to \phi K^0_L$. Solid curves show the fit to signal plus background distributions, and dashed curves show the background contributions.

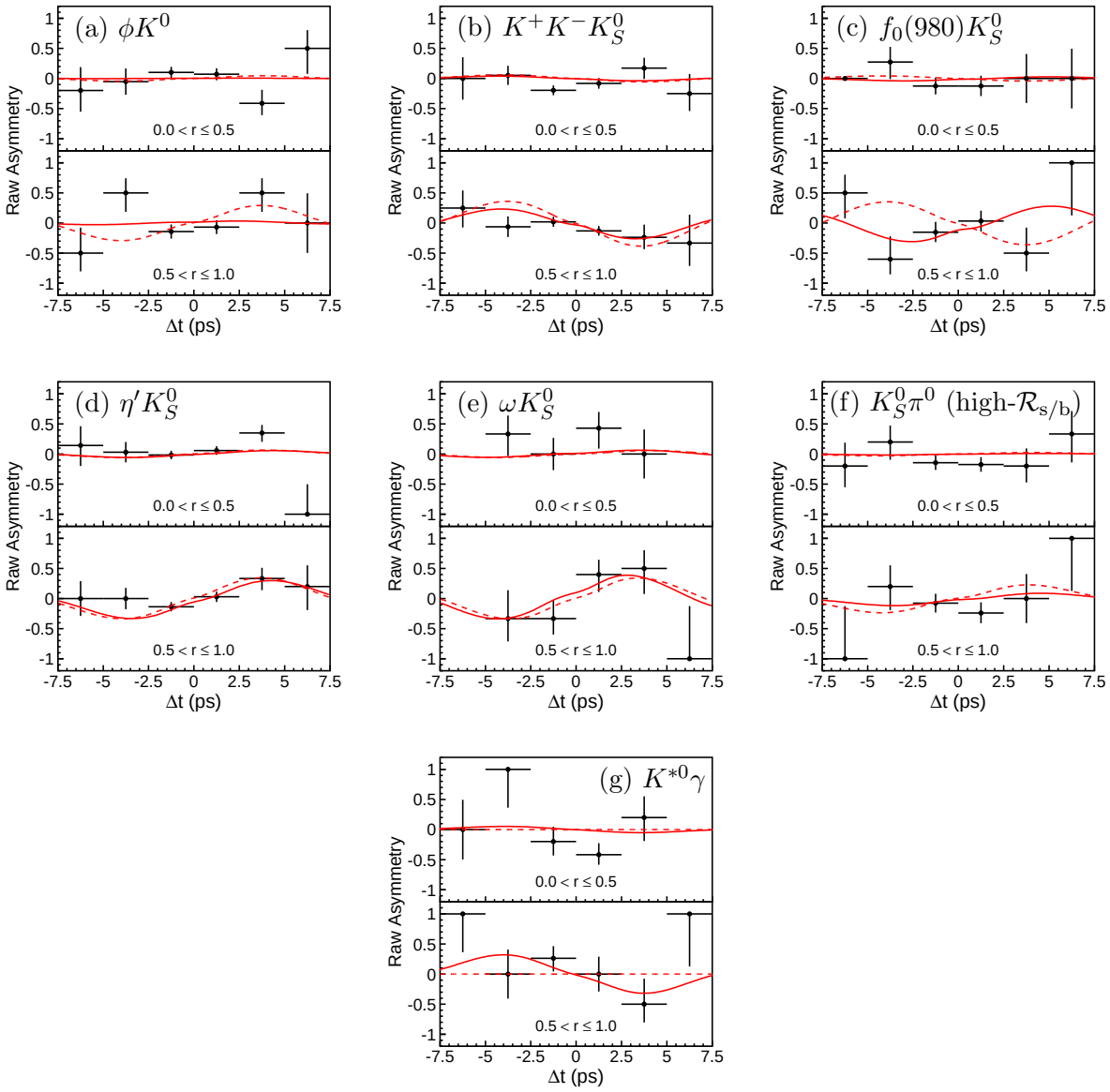

FIG. 2: The asymmetry, A, in each Δt bin with $0 < r \leq 0.5$ (top) and with $0.5 < r \leq 1.0$ (bottom) for (a) $B^0 \to \phi K^0$, (b) $B^0 \to K^+K^-K^0_S$, (c) $B^0 \to f_0(980)K^0_S$, (d) $B^0 \to \eta' K^0_S$, (e) $B^0 \to \omega K^0_S$, (f) $B^0 \to K^0_S\pi^0$ (for the high-$\mathcal{R}_{s/b}$ region only), and (g) $B^0 \to K^{*0}\gamma$. The solid curves show the result of the unbinned maximum-likelihood fit. The dashed curves show the SM expectation with $\sin 2\phi_1 = +0.73$ ($\mathcal{S} = 0$ for $B^0 \to K^{*0}\gamma$) and $\mathcal{A} = 0$.

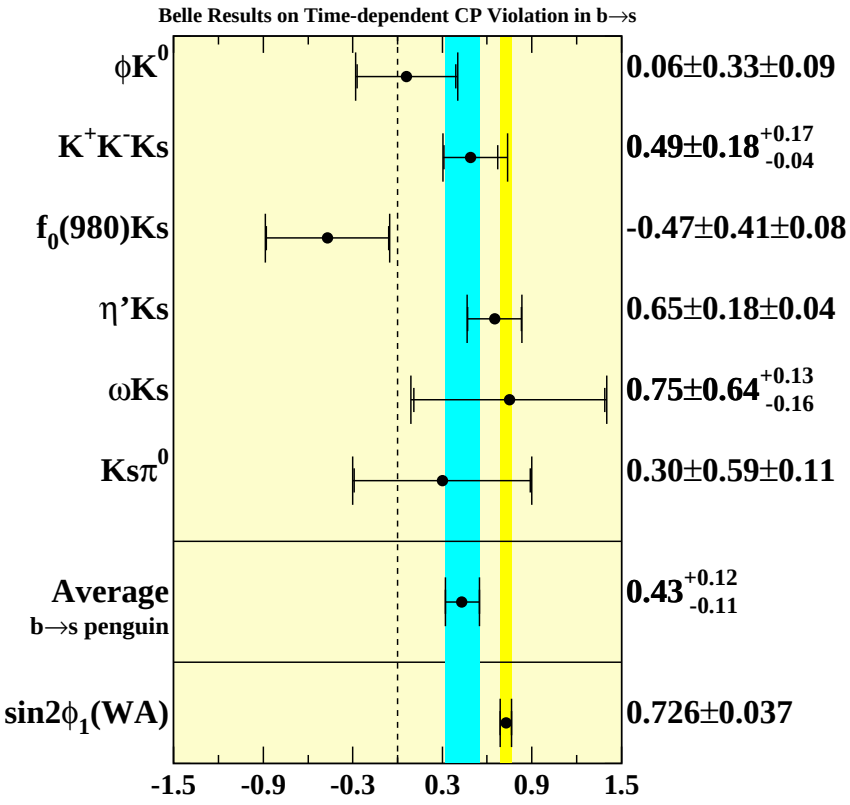

FIG. 3: Summary of $\sin 2\phi_1$ measurements performed with B^0 decay governed by the $b \to s\overline{q}q$ transition. The world-average $\sin 2\phi_1$ value obtained from $B^0 \to J/\psi K^0$ and other related decay modes governed by the $b \to c\overline{c}s$ transition [6] is also shown as the SM reference.